scientific reports

OPEN

Sequestration of gene products by decoys enhances precision in the timing of intracellular events

Kuheli Biswas[1✉], Supravat Dey[2✉] & Abhyudai Singh[3✉]

Expressed gene products often interact ubiquitously with binding sites at nucleic acids and macromolecular complexes, known as decoys. The binding of transcription factors (TFs) to decoys can be crucial in controlling the stochastic dynamics of gene expression. Here, we explore the impact of decoys on the timing of intracellular events, as captured by the time taken for the levels of a given TF to reach a critical threshold level, known as the *first passage time* (FPT). Although nonlinearity introduced by binding makes exact mathematical analysis challenging, employing suitable approximations and reformulating FPT in terms of an alternative variable, we analytically assess the impact of decoys. The stability of the decoy-bound TFs against degradation impacts FPT statistics crucially. Decoys reduce noise in FPT, and stable decoy-bound TFs offer greater timing precision with less expression cost than their unstable counterparts. Interestingly, when both bound and free TFs decay at the same rate, decoy binding does not directly alter FPT noise. We verify these results by performing exact stochastic simulations. These results have important implications for the precise temporal scheduling of events involved in the functioning of biomolecular clocks, development processes, cell-cycle control, and cell-size homeostasis.

Sequestration of gene products at genomic sites and in phase-separated particles critically shapes the stochastic dynamics of biomolecular circuits defining cellular responses to diverse stimuli[1–6]. For example, transcription factors (TFs) not only bind to their target promoters but also bind promiscuously to "decoy sites" scattered across the genome[7–9]. When binding to such decoys stabilizes an otherwise actively degraded TF, decoys have been shown to buffer stochastic variation in the levels of free (unbound) TF[10–12]. In contrast, when binding does not impact TF stability, decoys can function as noise amplifiers[13]. This latter scenario can occur for stable TFs whose concentrations are diluted from cellular growth.

While both experimental and computational works have explored the effects of sequestration mechanisms on stochastic variation in gene product levels, their impact on event timing remains mostly unexplored. Some theoretical and computational works have shown that the sequestration of TFs with decoys plays diverse roles in controlling the mean and stochastic dynamics in various genetic circuits such as oscillators[14–19] and toggle switches[19]. Recent studies have shown that decoy binding can crucially affect an event's mean first passage time (FPT) in auto-regulatory circuits[20], and play an important role in precision control of bacterial replication initiation[21]. In this contribution, we explore the influence of decoys in the timing noise of events, employing FPT formalism. This analysis considers events triggered by the accumulation of a specific protein to a predefined threshold level. Several works have derived analytical expressions for FPT statistics for different models of stochastic gene expression, including models with feedforward and feedback regulation[22–25], post-transcriptional regulation[26,27], miRNA-mediated regulation of protein translation[28], providing rich insight into event timing in the context of different biological phenomena such as cell-cycle regulation[29], lysis timing of phages[30–32], development[33], cell-state transitions[34,35], and neuronal firing of action potentials[36,37]. Here we systematically explore how decoy-based sequestration of gene products impacts stochasticity in FPT using well-established analytical approximations corroborated with exact stochastic simulations.

Understanding the variability in the timing of gene expression is crucial for unraveling fundamental biological mechanisms at the single-cell level. Identifying the regulatory strategies that can modulate this variability is essential for decoding the underlying design principles of cellular regulatory networks that govern timing.

[1]Department of Chemical Engineering, Network Biology Research Lab, Technion, Israel Institute of Technology, Haifa, Israel. [2]Department of Physics and Department Computer Science and Engineering, SRM University - AP, Amaravati, Andhra Pradesh 522240, India. [3]Department of Electrical and Computer Engineering, Biomedical Engineering, Mathematical Sciences, Center for Bioinformatics and Computational Biology, University of Delaware, Newark, DE 19716, USA. ✉email: kuhelibiswas@campus.technion.ac.il; supravat.dey@gmail.com; absingh@udel.edu

Advancements in experimental techniques, notably fluorescence time-lapse microscopy, often integrated with microfluidic platforms to maintain cells in a precisely controlled environment across multiple generations, are poised to significantly enhance data accessibility on gene expression timing and its variabilities. Consequently, a robust theoretical framework elucidating the dynamics of timing fluctuations is imperative. Such a framework is necessary to effectively interpret forthcoming data, guide the development of targeted experimental designs, and facilitate the engineering of synthetic biological circuits with tailored timing characteristics.

Materials and methods
Model formulation
To analytically explore the impact of decoy binding on FPT statistics, we consider TF synthesizing in stochastic bursts (Fig. 1). Such bursty gene expression is experimentally observed across various cell types due to different transcriptional and translational mechanisms[38–47]. For example, in eukaryotes, a promoter may randomly switch from an inactive to an active state, produce bursts of mRNA, and quickly turn off, with the burst rate determined by the switching rate to the active state[48–50]. Assuming short-lived mRNAs in prokaryotes, each mRNA degrades rapidly after translating a burst of proteins, with the burst rate equal to the transcription rate[51–55]. We model the combined effects of transcriptional and translational bursts by assuming Poisson arrival of burst events with a rate k, where each event creates B molecules[12,13]. The burst size B is an independent and identically distributed non-negative random variable following an arbitrary distribution. However, for plotting and simulation purposes where we consider a geometrical distribution grounded in prior research[53,56–58]. A TF molecule then decays with rate γ_f.

An expressed TF molecule binds reversibly to a decoy from a pool of total N decoy sites to form a decoy-bound complex. The genomic decoys are the numerous high-affinity binding sites where TFs bind independently without any direct functional consequences[8]. The binding and unbinding rates are k_b and k_u, respectively. The total decoy number N is kept fixed in our study. Experimental evidence suggests that the decay of decoy-bound TFs is context-dependent. For some TFs such as p53[59] and MyoD[60], the decoy binding protects TFs from degradation. While some other TFs decoy-binding promotes degradation such as VP16 in *Saccharomyces cerevisiae* via ubiquitin-mediated proteolysis[61]. It has been shown theoretically that the stability of bound TFs plays crucial roles in the deterministic and stochastic dynamics of the nonregulatory[13], auto-regulatory[10], and oscillatory gene circuits[17]. Here, we assume the degradation of a TF molecule in the bound state is $\beta\gamma_f$. We will focus on two values of $\beta=1$ and 0, where $\beta=0$ corresponds to no decay of bound TF, and $\beta=1$ corresponds to equal degradation rates for both the free and bound TF.

Our TF expression and sequestration model at decoy binding sites is based on the standard stochastic formulation of chemical kinetics[62,63]. The model is comprised of five following events that occur probabilistically at exponentially distributed time intervals

$$\text{TF synthesis:} \quad Prob(x_f(t + dt) = x_f(t) + i) = k\alpha_x(i)dt, \tag{1a}$$

$$\text{TF binding:} \quad Prob(x_f(t + dt) = x_f(t) - 1, x_b(t + dt) = x_b(t) + 1) = k_b x_f(N - x_b)dt, \tag{1b}$$

$$\text{TF unbinding:} \quad Prob(x_f(t + dt) = x_f(t) + 1, x_b(t + dt) = x_b(t) - 1) = k_u x_b(t)dt, \tag{1c}$$

$$\text{Free TF degradation:} \quad Prob(x_f(t + dt) = x_f(t) - 1) = \gamma_f x_f(t)dt, \tag{1d}$$

$$\text{Bound TF degradation:} \quad Prob(x_b(t + dt) = x_b(t) - 1) = \beta\gamma_f x_b(t)dt, \tag{1e}$$

where $\alpha_x(i)$ is the probability distribution for burst size $B = i$. $x_f(t)$, $x_b(t)$ and $x(t) := x_f(t) + x_b(t)$ denote the level of free, bound and total (free + bound) TF at time t inside the cell, respectively. To study the role of decoy binding sites on the statistics of event timing, we characterize the dynamical moments of free TF numbers as a function of the number of decoy sites N. The first and second moments of a stochastic variable Y at time t are denoted as $\langle Y \rangle$ and $\langle Y^2 \rangle$, respectively. The angular bracket $\langle \cdot \rangle$ represents ensemble averages, which are obtained by averaging over many trajectories in simulations. The noise in Y is quantified by its coefficient of variation square at time t, which is denoted by CV_Y^2. For readers' convenience, we provide a list of model parameters and their description in Table 1.
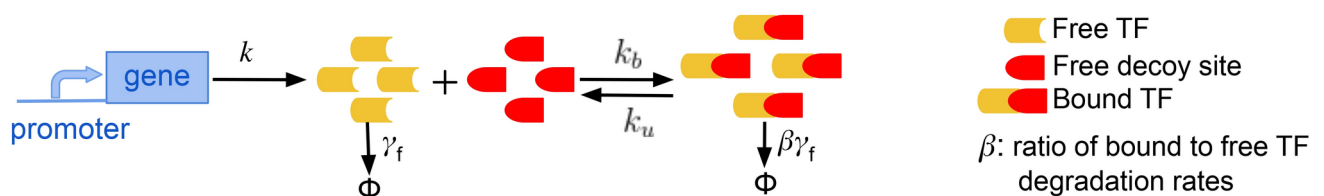

Fig. 1. Schematic of TF synthesis model in the presence of decoy binding sites. The synthesis of free TFs occurs in stochastic bursts with rate k, which reversibly bind/unbind to N decoy binding sites with rates k_b and k_u. Both the free and bound TFs are subject to degradation with rates γ_f and $\beta\gamma_f$, respectively.

Symbol	Description	Symbol	Description
k	TF burst frequency	B	TF bust size
k_b	TF binding rate	k_u	TF unbinding rate
k_d	Dissociation constant (k_u/k_b)	γ_f	Free TF degradation rate
$\beta\gamma_f$	Bound TF degradation rate	N	Total decoy binding sites
x_f	Free TF number at time t	$\langle Y \rangle$	Mean value at time t
x_b	Bound TF number at time t	CV_Y	Coefficient of variation of Y at time t
x	Total TF number $(x_f + x_b)$ at time t	X	Threshold number of free TFs
T	First passage time	$\mathcal{T}$	$:= \gamma_f T$ FPT in the dimensionless unit
x_0	$:= k\langle B\rangle/\gamma_f$, The stead-state mean of TF numbers for no decoy, $N = 0$		
g	$g(X, N, k_d)$, fraction of free TFs in total TFs at threshold crossing		

Table 1. Summary of notation used.

Based on the above discrete-state continuous-time Markov model (1), one can write a corresponding Chemical Master Equation (CME) that provides the time evolution of the joint probability density function[64]. However, an exact solution of the CME is analytically intractable. Taking an alternative approach, we focus on the statistical moments of the molecular counts and use the well-known Linear Noise Approximation (LNA)[65–69] to obtain closed-form formulas for the mean and noise level dynamics (see Supplementary B).

FPT statistics in the absence of decoys
The first passage time or event timing in our study is defined as the minimum time required for the free TF level to reach a critical threshold for the first time to trigger some downstream processes. More precisely, starting from zero initial conditions, the FPT is mathematically described by the following random variable

$$T := \inf\{t : x_f(t) \geq X | x_f(0) = 0\}, \tag{2}$$

where X is the critical threshold level of free TFs needed for some events to occur. The FPT is a stochastic variable since the free TF number fluctuates over time. When the fluctuations in the free TF level are small, the mean FPT, $\langle T \rangle$ is approximately the time required for the mean free TF level to reach the threshold for the first time, i.e.,

$$\langle T \rangle \approx \{t | \langle x_f(t) \rangle = X\}. \tag{3}$$

In the absence of decoys, the mean dynamics of free TFs are usually straightforward to obtain from linear biochemical systems given as follows[51]

$$\langle x_f \rangle = x_0 \left(1 - e^{-\tau}\right), \tag{4}$$

which increases monotonically with time, asymptotically approaching the steady-state value $x_0 := k\langle B\rangle/\gamma_f$. For simplicity, we use dimensionless time, $\tau = \gamma_f t$, implying time measurement in the unit of lifetime of a free TF molecule.

The noise in FPT is quantified by the squared coefficient of variation (CV_T^2), which is the ratio of the variance and the mean squared in FPT. By using the small noise approximation (SNA) in free TF level, one can compute the FPT noise as follows (see Supplementary A).

$$CV_T^2 = \frac{\langle T^2 \rangle - \langle T \rangle^2}{\langle T \rangle^2} \approx \left[CV_{x_f}\left(S_{x_f}\right)^{-1}\right]^2_{t=\langle T \rangle}, \tag{5}$$

where

$$S_{x_f} := \frac{d\langle x_f \rangle}{dt}\frac{t}{\langle x_f \rangle} = \frac{d\log\langle x_f \rangle}{d\log(t)}, \tag{6}$$

is the dimensionless log sensitivity of the mean free TF level with respect to time. In the absence of decoys, the noise dynamics of free TFs is given as follows[51]

$$CV_{x_f}^2 = \frac{1}{2\langle x_f \rangle}\left[\frac{\langle B^2 \rangle}{\langle B \rangle}\left(1 + e^{-\tau}\right) + (1 - e^{-\tau})\right], \tag{7}$$

which asymptotically reaches the steady-state value $\langle B^2 \rangle / \langle B \rangle x_0$. We note that Eq. (5) leads to the same mathematical expression as in Ref.[70] obtained by a different approach by following the simple geometric argument in TF number dynamics.

Now, using the dynamics of mean and noise of free TFs in the definition of mean FPT (Eq. 3) and FPT noise (Eq. 5) one can obtain

$$\langle \mathscr{T} \rangle = -\ln\left[1 - \frac{X}{x_0}\right], \tag{8}$$

$$CV_T^2 = \frac{\left(1 - e^{-\langle \mathscr{T} \rangle}\right)}{2x_0(\langle \mathscr{T} \rangle e^{-\langle \mathscr{T} \rangle})^2}\left[\frac{\langle B^2 \rangle}{\langle B \rangle}\left(1 + e^{-\langle \mathscr{T} \rangle}\right) + (1 - e^{-\langle \mathscr{T} \rangle})\right], \tag{9}$$

which is the same expression as in the Ref.[70]. We use mean FPT in the dimensionless unit $\langle \mathscr{T} \rangle = \gamma_f \langle T \rangle$. One significant feature emerges from Eq. (9) is that FPT noise exhibits a nonmonotonic behavior with mean FPT and the optimal value of normalized mean FPT is $\mathscr{T} \approx 0.79$ for geometric burst size distribution with large average burst size [70]. The identification of the optimal threshold or mean FPT at $\mathscr{T} \approx 0.79$ is further substantiated by recent theoretical advances, where the lysis time has been analytically modeled within the FPT framework[71]. Their precise analytical calculations, devoid of any approximations, are in remarkable agreement with the experimental measurements of lysis times observed in variants of λ phages[31].

FPT statistics in the presence of decoys

In the presence of decoys, the average dynamics for free and bound TF numbers are nonlinear and can be expressed as follows

$$\frac{d\langle x_f \rangle}{dt} = k\langle B \rangle + k_u\langle x_b \rangle - k_b(N - \langle x_b \rangle)\langle x_f \rangle - \gamma_f\langle x_f \rangle, \tag{10}$$

$$\frac{d\langle x_b \rangle}{dt} = -k_u\langle x_b \rangle + k_b(N - \langle x_b \rangle)\langle x_f \rangle - \beta\gamma_f\langle x_b \rangle. \tag{11}$$

The same closed-form mean dynamics can be derived from the chemical master equation corresponding to the model in (1) by applying the linear noise approximation (LNA)[12,13]. A direct consequence of using the LNA is that the time evolution of the means matches the deterministic chemical rate equations. The nonlinearity in the dynamics of free and decoy-bound TFs makes calculating FPT statistics challenging. However, as we will see below, in some limits one can bypass this nonlinearity by considering the dynamics of total TFs, $x = x_f + x_b$ as follows

$$\frac{d\langle x \rangle}{dt} = k\langle B \rangle - \gamma_f(\langle x_f \rangle + \beta\langle x_b \rangle), \tag{12}$$

and reformulating the FPT question in terms of total TFs. For example, the above mean dynamics of the total TF number becomes linear for $\beta = 1$.

Generally binding/unbinding happens at faster rates compared to synthesis and degradation rates, i.e., the timescales for binding/unbinding are much shorter. In this limit, the dynamics of binding unbinding reaches a quasi-static equilibrium (QSE) and obeys the following relationship: $k_u x_b = k_b(N - x_b)x_f$. This QSE or adiabatic limit is a prevalent approach in gene expression modeling[72–74], supported by recent experimental evidence[75]. Using this approximation we get the relation between total and free TF numbers as follows

$$\frac{x_f}{x} = \frac{x_f + k_d}{x_f + N + k_d} \equiv g(x_f, N, k_d), \tag{13}$$

where $0 \leq g(x_f, N, k_d) \leq 1$ and it signifies the fraction of free TF molecules. For notational convenience, we use $g(X, N, k_d)$ as g henceforth.

Based on Eq. (13) we reformulate the FPT in terms of the dynamics of the total TF level. Instead of locating the time for the free TF level to reach a threshold X for the first time, we find the time when the total TF level first time hits a normalized threshold X/g. More precisely, the modified FPT is mathematically described by the following random variable

$$T :\approx \inf\{t : x(t) \geq X/g | x(0) = 0\}. \tag{14}$$

We numerically demonstrate that this assumption works well when the noise in the system is relatively small. In Fig. 2, we have plotted the simulated trajectories and distributions of actual FPT (Eq. 2) and modified FPT (Eq. 14). Not only the mean FPT (Fig. 2a,b), but the full distributions of FPT (Fig. 2c,d) from these two definitions appear to be identical. This approximation even persists when the binding/unbinding reactions are slow, of the order of TF degradation rate (see Supplementary Fig. S1). However, in the limit of a small free TF
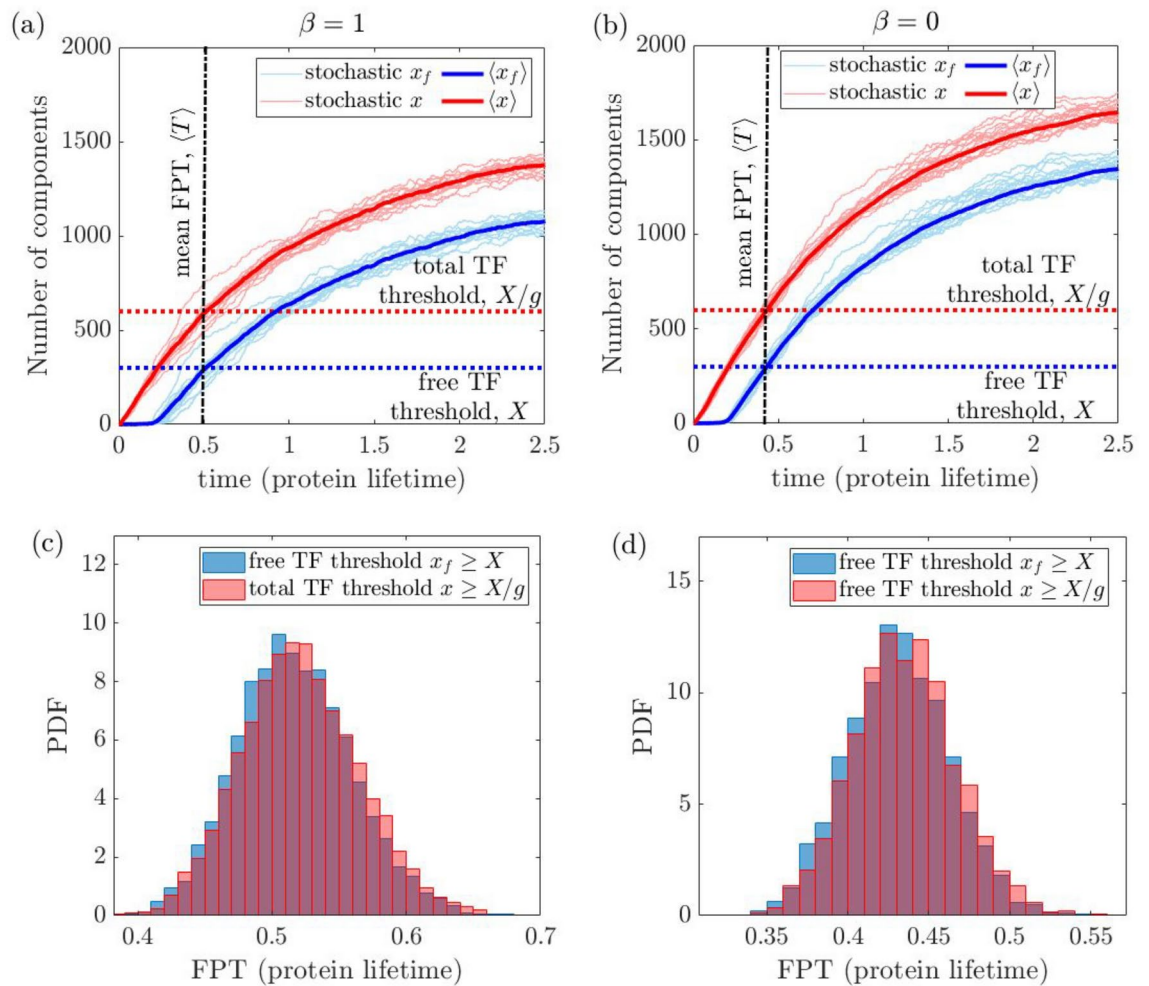
Fig. 2. FPT statistics of free TF level reaching a threshold X is approximated by FPT statistics of total TF level reaching a normalized threshold X/g. Simulated stochastic and mean trajectories of total (x) and free (x_f) TFs for **(a)** $\beta = 1$ and **(b)** $\beta = 0$ along with threshold of x_f is X and x is X/g. Simulated FPT distributions from both thresholds in Eqs. (2) and (14) will show a significant overlap for **(c)** $\beta = 1$ and **(d)** $\beta = 0$. We assume the shifted geometric distribution of burst size, i.e., $\langle B^2 \rangle = 2\langle B \rangle^2 + \langle B \rangle$ with parameter values: $N = 300$, $X = 300$, $\gamma_f = 1\ hr^{-1}$ per TF molecule, $k_b = k_u = 50\ hr^{-1}$ per pair molecules, $\langle B \rangle = 10$, $x_0 = 1500$. We use the stochastic simulation algorithm (SSA)[76] over 5×10^3 realizations on model Eq. (1).

threshold, $X \ll x_0$ these two distributions deviate from each other, and the approximation is no longer valid (see Supplementary Fig. S2).

Following the same SNA approximation in x as mentioned before in Eq. (3), we can write the modified mean FPT as

$$\langle T \rangle \approx \{t|\langle x(t)\rangle = X/g\}. \tag{15}$$

Similar to Eq. (5), the FPT noise will be as follows

$$CV_T^2 \approx \left[CV_x\left(S_x\right)^{-1}\right]_{t=\langle T \rangle}^2 \qquad S_x := \frac{d\log\langle x\rangle}{d\log(t)}, \tag{16}$$

which depends on the noise dynamics of total TFs (CV_x^2) and the dimensionless log sensitivity of the mean total TF level with respect to time (S_x) (see Supplementary Sect. A). So, using SNA and fast binding/unbinding approximations, we can obtain analytical expressions for the mean and noise of free TFs' FPT from the total TFs' moment dynamics. Next, we will focus on two key regimes characterized by $\beta=0$ implying stable decoy-bound TFs and $\beta=1$ indicating the same degradation rate of free and decoy-bound TFs.

Results
FPT statistics when both bound and free TFs decay at the same rate ($\beta = 1$)

Using $\beta=1$ in Eq. (12) one can obtain the average dynamics of the total TF number, which is the same as the dynamics of average TF number for no decoy (Eq. 4). Now using the modified definition of mean FPT in Eq. (15), one can obtain an expression from mean FPT as follows

$$\langle \mathscr{T} \rangle = - \ln \left[1 - \frac{X}{gx_0} \right], \tag{17}$$

which reduces to Eq. (8) for no decoys as the fraction of free TFs $g=1$ when $N=0$. The mean FPT increases monotonically with N and diverges for large N as $g \rightarrow 0$ when $N \rightarrow \infty$ (Fig. 3a). The analytical form of mean FPT obtained by using the modified threshold on total TFs (Eq. 15) agrees well with the exact stochastic simulation algorithm (SSA)[76] (see Fig. 3a) of the decoy model in Eq. (1) that considers the actual free TF number threshold (Eq. 2).

Now, for the analysis of the FPT noise of free TF, we need the noise dynamics of the total TF number as mentioned in Eq. (16). In the limit of $\beta=1$, the noise in total TF numbers is the same as no decoy case, which is given in Eq. (7) (see Supplementary Sect. B). Using the expressions of mean and noise dynamics of total TF numbers in Eq. (16) one can obtain the mathematical form of FPT noise as follows
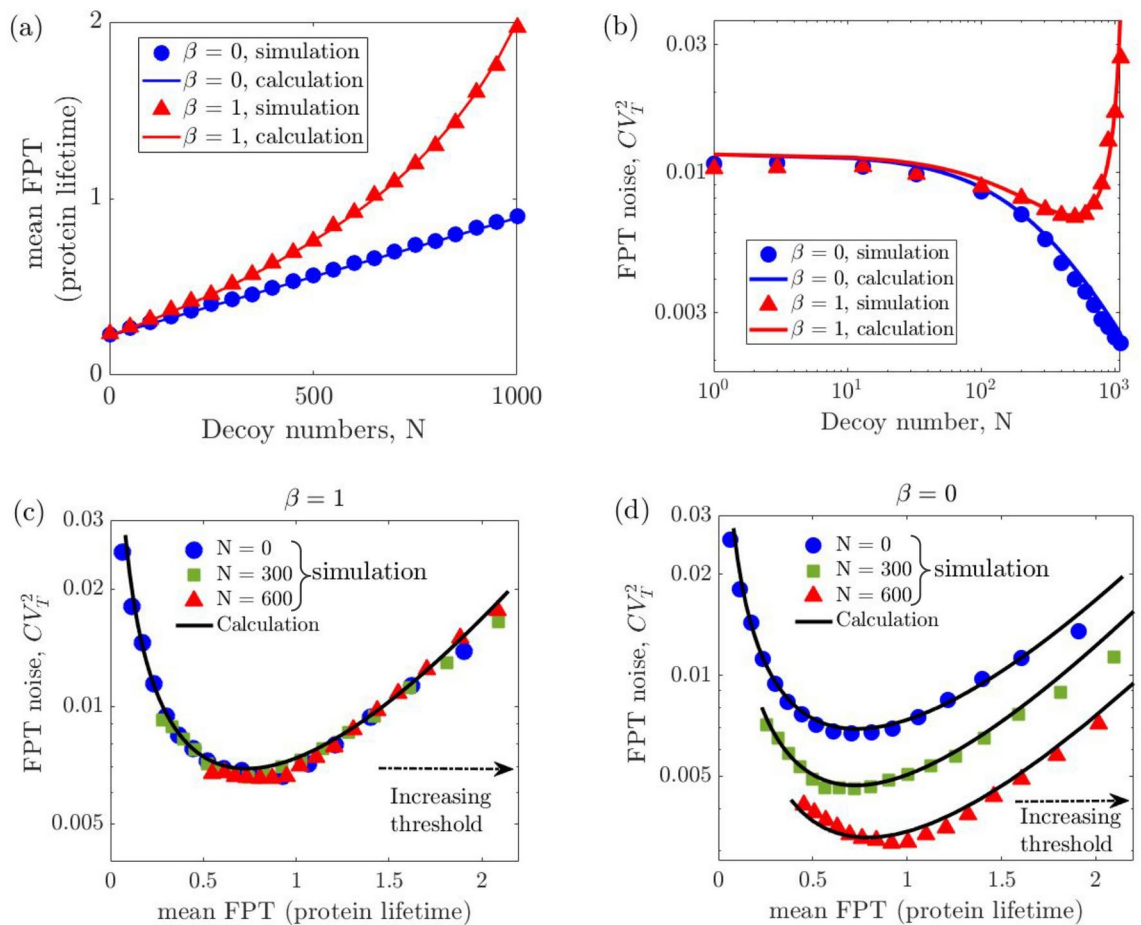

Fig. 3. Stability of bound TFs distinctly influences the FPT statistics. Variation of **(a)** mean FPT and **(b)** FPT noise with decoy number for $\beta = 1$ Eqs. (17), (18) (red triangles) and $\beta = 0$ Eqs. (20), (22) at fixed threshold value $X = 300$. Variation of FPT noise with mean FPT for **(c)** $\beta = 1$ and **(d)** $\beta = 0$ for three different values of N; $N = 0$, 300, and 1000. For $\beta = 1$, the relation between $\langle T \rangle$ and CV_T^2 follows a master curve (Eq. 18) for all N values, which deviates for $\beta = 0$, for nonzero N values (Eq. 22). For the simulation, we use the stochastic simulation algorithm (SSA)[76] over 5×10^3 realizations using Eqs. (1), and (2). For each N, we change the value of $\langle T \rangle$ by changing the threshold X. We assume the shifted geometric distribution of burst size, i.e., $\langle B^2 \rangle = 2\langle B \rangle^2 + \langle B \rangle$ with parameter values: $\gamma_f = 1 \ hr^{-1}$ per TF molecule, $k_b = k_u = 50 \ hr^{-1}$ per pair molecule, $\langle B \rangle = 10$, $x_0 = 1500$.

$$CV_T^2 = \frac{\left(1 - e^{-\langle \mathscr{T} \rangle}\right)}{2x_0(\langle \mathscr{T} \rangle e^{-\langle \mathscr{T} \rangle})^2} \left[\frac{\langle B^2 \rangle}{\langle B \rangle}(1 + e^{-\langle \mathscr{T} \rangle}) + (1 - e^{-\langle \mathscr{T} \rangle}) \right],$$ (18)

which is the same as Eq. (9) for no decoy case. In Eq. (18), CV_T^2-a measure of FPT noise-implicitly depends on N via $\langle \mathscr{T} \rangle$. This implies that the relation between the FPT mean and noise remains invariant of N when $\beta=1$ as presented in Fig. 3c. So, for $\beta=1$, with different N values, $\langle T \rangle$ and hence CV_T^2 will change in such a way that it will follow a master curve, which is Eq. (18). It is remarkable to note that despite the influence of decoy binding on the dynamics of free TFs, it does not modify the relationship between the FPT mean and noise. The optimal value of mean FPT is $\langle \mathscr{T} \rangle \approx 0.79$, similar to the no decoy case as mentioned before in ("FPT statistics in the absence of decoys" section). The approximated FPT noise from our analysis agrees well with the exact SSA[76]. Increasing the number of decoys results in a higher mean FPT (Fig. 3a) and thus impacts the FPT noise according to Eq. (18). The dependence of FPT noise on the number of decoys is depicted in Fig. 3b.

FPT statistics when bound TFs are protected from degradation ($\beta = 0$)

Using $\beta=0$ in Eq. (12) one cannot exactly solve the differential equation for $\langle x \rangle$. However, in the limit of $k_d \ll x_f$, i.e., when all decoy sites are bound with TFs ($x_b \approx N$) one can get an approximated dynamics of the total TF number as follows

$$\langle x \rangle = (x_0 + N)\left(1 - e^{-\tau}\right),$$ (19)

which is the same as the dynamics of the free average TF number for $N=0$ (Eq. 4). Now using the modified definition of FPT in Eq. (15), one can obtain an expression from mean FPT as follows

$$\langle \mathscr{T} \rangle = -\ln\left[1 - \frac{X}{g(x_0 + N)}\right],$$ (20)

which reduces to Eq. (8) for no decoys. For $\beta=0$, though the mean FPT increases with N, it does not show a diverging trend like $\beta=1$ (Eq. 17) as $g(x_0 + N) \to (X + k_d)$ when $N \to \infty$. Our approximated calculation for the mean FPT in Eq. (20) agrees well with the stochastic simulation algorithm (SSA)[76] of the decoy model in Eq. (1) (Fig. 3a).

Now, for the analysis of noise in free TF numbers' FPT, we need the noise dynamics of the total TF number as mentioned before in Eq. (16). In the limit of $\beta=0$, the noise in total TF numbers is given as follows (see Supplementary Sect. B)

$$CV_x^2 = \frac{1}{2\langle x \rangle}\left[\frac{1}{x_0 + N}\left(x_0\frac{\langle B^2 \rangle}{\langle B \rangle} + N\right)(1 + e^{-\tau}) + (1 - e^{-\tau})\right],$$ (21)

which converges to Eq. (7) for $N=0$. Using the expressions of $\langle x \rangle$ (Eq. 19) and CV_x (Eq. 21) in Eq. (16) one can obtain the mathematical form of FPT noise as follows

$$CV_T^2 = \frac{\left(1 - e^{-\langle \mathscr{T} \rangle}\right)}{2(x_0 + N)(\langle \mathscr{T} \rangle e^{-\langle \mathscr{T} \rangle})^2}\left[\frac{1}{x_0 + N}\left(x_0\frac{\langle B^2 \rangle}{\langle B \rangle} + N\right)(1 + e^{\langle \mathscr{T} \rangle}) + (1 - e^{-\langle \mathscr{T} \rangle})\right],$$ (22)

which is an explicit function of N, unlike for the case of $\beta=1$ in Eq. (18). The variation of FPT noise with decoys is shown in Fig. 3b. Equation (22) demonstrates that the relationship between the FPT mean and noise deviates from the master curve observed in the absence of decoys as CV_T^2 is inversely proportional to the number of decoys (N). This analysis is also supported by the stochastic simulation algorithm (SSA) results shown in Fig. 3d.

FPT noise for a fixed mean FPT

In the previous section, we observe how the decoys alter both the mean FPT and the noise for a given production rate, decay rate, and binding affinity of transcription factors. The response of living cells to the presence of decoys influencing event timing remains unclear. It can be hypothesized that cells may maintain a constant mean FPT. In this section, we explore the behavior of FPT noise while holding the mean FPT constant. Consequently, to keep the mean FPT constant while varying N, it becomes necessary to modify certain parameters as $\langle \mathscr{T} \rangle = f(N, X, x_0, k_d)$ (Eqs. 17, 20 for $\beta=1$ and 0). Here, we focus on adjusting burst frequency (k) hence $x_0(= k\langle B \rangle/\gamma_f)$ and threshold (X). However, increasing burst frequency results in a higher load of TFs in the cell. Similarly, raising the threshold level leads cells to produce more TFs. Therefore, enhancing both the burst frequency and the threshold level increases the TF load on the cell, which we describe qualitatively as being more "expression cost" for the cell. Moving forward, we will explore how variations in burst frequency and threshold influence the timing precision of cellular processes, particularly in scenarios involving the presence of decoys, for both $\beta=1$ and 0.

First, we focus on tuning the threshold, X to maintain a fixed mean FPT. For both β values, the threshold decreases linearly with increasing decoys (Fig. 4b). A reduced threshold requirement means fewer TFs need to be produced, implying lesser expression cost for cells. Moreover, when $\beta=0$, it can be seen from Eq. (22) CV_T^2 monotonically decays with N and asymptotically follows a $1/N$ relationship (Fig. 4a). Therefore, for stable decoy-
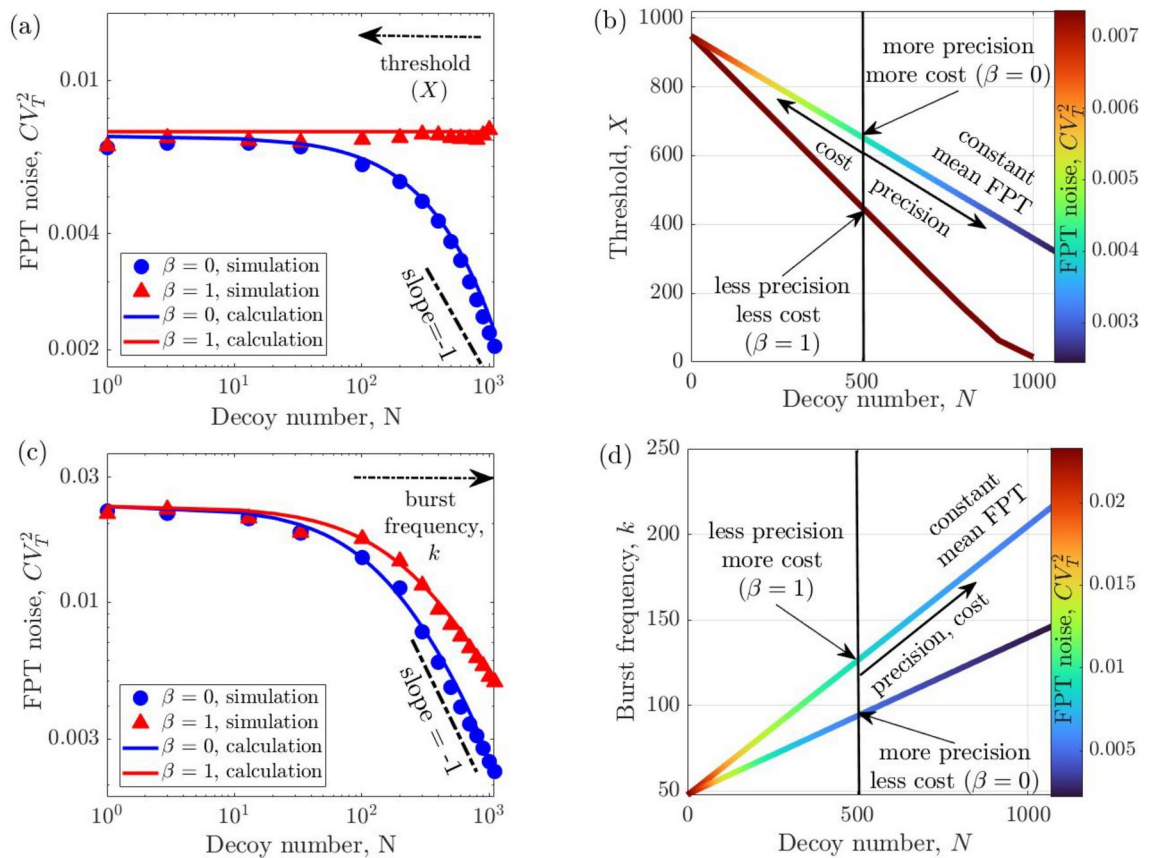
Fig. 4. Decoys enhance timing precision at the expense of higher expression cost for a fixed mean FPT. Variation of the FPT noise with decoy number for fixed $\langle \mathscr{T} \rangle = 1$ by changing **(a)** threshold for a fixed burst frequency $k = 150$ and varying **(c)** burst frequency for a constant threshold $X = 300$. For **(a,c)** we tune, respectively, X and k by using Eq. (17) for $\beta = 1$ and Eq. (20) for $\beta = 0$. The parameters used for figures: $\gamma_f = 1\ hr^{-1}$ per TF molecule, $k_b = k_u = 50\ hr^{-1}$ per pair molecule, $\langle B \rangle = 10$. We use the SSA[76] over 5×10^3 realizations for simulation. Contours representing a constant mean FPT of 1 in the **(b)** $N - X$ and **(d)** $N - k$ plane are depicted for $\beta = 1$ and $\beta = 0$. The contours are color-coded by CV_T^2 quantifying FPT noise levels. Precision increases in the direction of the arrow, indicating lesser noise. On the same contour, higher thresholds and burst frequency increase "expression costs" due to elevated TF loads. While not quantified, the expression cost qualitatively increases in the direction of the arrow.

bound TFs ($\beta = 0$), decoy binding enhances both precision and cost-effectiveness for cells, provided the threshold is tuned to keep the mean FPT constant (see Fig. 4b). In contrast, for $\beta = 1$, the noise in FPT is maintained at the same level observed without decoys, regardless of the increase in N as seen in Fig. 4a. This outcome occurs as CV_T^2 in Eq. (18) implicitly depends on X and N through $\langle T \rangle$, which is kept fixed.

Next, we focus on tuning burst frequency to maintain a constant mean FPT fixed for varying values of N. Using the mean FPT equations for $\beta = 1$ (Eq. 17) and $\beta = 0$ (Eq. 20), we can precisely determine x_0 and, subsequently, the burst frequency, $k = x_0 / \langle B \rangle$ for a fixed mean FPT while N is changing. For both scenarios, the burst frequency increases linearly with N, as shown in Fig. 4d. This increase in burst frequency increases transcription cost[77] hence expression cost. Moreover, linearly increasing burst frequency with decoy numbers reduces FPT noise as CV_T^2 inversely correlates with burst frequency both for $\beta = 1$ (Eq. 18) and $\beta = 0$ (Eq. 22). Hence FPT noise decays as $1/N$ when we tune burst frequency to maintain a fixed mean FPT. The exact analytical forms of CV_T^2 for both β values are plotted in Fig. 4c, which have -1 slope in the log-log axes (black dashed line for the eye guide). Our approximated analytical calculation matches the exact stochastic simulations[76] of the model described in Eqs. (1) and (2). Therefore, decoy binding enhances timing precision at the expense of higher expression cost (see Fig. 4d). However, for a specific number of decoy binding sites (N), stable bound TFs ($\beta = 0$) offer greater timing precision with lower expression costs compared to unstable bound TFs ($\beta = 1$) as detailed in Fig. 4d.

Discussion
In this study, we have systematically investigated how sequestration of TFs by decoy sites impacts the statistics of event timing, a scenario not extensively explored in the existing literature. Specifically, we have studied the first passage time (FPT) statistics, the time required for free TF numbers to cross a certain threshold value. We have obtained approximated analytical expressions for the mean and noise of FPT. The noise is quantified by the

square of the coefficient of variation (CV_T^2) in FPT. As the decoy binding introduces nonlinearity, the analytical tractability of the problem usually becomes challenging, especially for the dynamics not only for the mean but also for the noise. Our analytical calculations of FPT moments are based on two key approximations: (1) quasi-static equilibrium (QSE), i.e., fast binding/unbinding reactions, and (2) small noise approximation (SNA) in TF levels. We have shown that we can eliminate nonlinearity by looking at the dynamics of the total TF level and reframing the FPT question in terms of the total TF level reaching an equivalent threshold. Our approximated simple analytical results provide better insights for understanding FPT noise and agree with exact stochastic simulations. Without decoys, the exact analytical calculations for FPT statistics are possible[31]. However, the complexity in the mathematical expression for exact formulas may prohibit simple intuitive insights that one achieves via SNA approximation[70]. While this contribution focuses on TFs binding to genomic decoy sites, this framework applies to other classes of proteins, for example, RNA-binding proteins binding to sites on RNA[78-80].

Our investigation indicates that the stability of decoy-bound TFs is critical in determining FPT statistics. Earlier studies have shown that stable bound TFs decrease gene expression variability at steady-state, whereas their degradation increases fluctuations[10,13]. In the context of biomolecular clocks, however, the degradation of bound TFs can enhance oscillatory behavior and reduce noise, while protecting these TFs from degradation can disrupt sustained oscillations in gene expression[17]. This study shows that the mean FPT increases with the number of decoy binding sites and this increment is rapid if bound TFs are unstable (Fig. 3a). Importantly, when the degradation rates for free and bound TFs are equal ($\beta=1$), FPT noise does not explicitly depend on the number of decoys but is influenced indirectly via the mean FPT. In this scenario, adjusting burst frequency (threshold) to maintain a constant mean FPT effectively reduces FPT noise (regulates) with decoys compared to the no-decoy scenario (see Fig. 4a,c). In contrast, for stable bound TFs ($\beta=0$), decoys consistently reduce FPT noise, as it directly correlates with the inverse function of the number of decoy sites (Eq. 22). On the other hand, while increasing decoys enhances the precision of event timing, it comes at the cost of a higher total protein load and consequently, increased expression cost.

The analytical formulas for the noise give theoretical insights into the role of decoys on the noise of FPT. These are derived by assuming small copy number fluctuations around the statistical mean and then taking fast bind/binding limit. Using numerical exact stochastic simulations, we have shown that the main results agree with the theory. The quantitative match between theory and simulations can be poor where the fluctuations are large. We numerically have found that results are not very sensitive to fast binding/unbinding limits (see Supplementary Fig. S3). Our model disregards explicit mRNA dynamics and considers only protein synthesis that occurs in bursts, which is valid when the mRNA lifetime is shorter than that of the protein. Considering explicit mRNA dynamics we numerically checked that the main results are consistent with our theoretical predictions (see Supplementary Fig. S4). It will also be interesting to consider different forms of parametric fluctuations coupled with intrinsically noisy expression, for example, the threshold level itself could be random in single cells[81], cell size varies over time, influencing both species number and concentration[82,83]. In our study, we assume that the number of total decoys is constant. However, genomic decoy numbers can fluctuate due to different DNA conformations and their dynamics[84]. Additionally, proteins that bind to TFs can act as decoys, such as those in biomolecular circuits associated with the heat-shock response[85,86]. The role of decoy number fluctuations in temporal precision would be a direction for future study. Another intriguing direction could involve the cooperative binding of TFs to decoy binding sites, which would cause the decoy binding rate to vary with the number of decoy-bound TFs.

Our novel finding of the dual role of decoys as noise regulators/buffers in event timing encourages more investigation into the regulatory function of decoys in complex gene networks. In our prior research, we used bacteriophage λ as a model system for studying event timing in individual cells. Here, an easily observable event (cell lysis) is the result of the expression and accumulation of a single protein (holin) in the *E. coli* cell membrane up to a threshold level[30,32,71], and precision in event timing is tied an optimal timing of phage-mediated cell lysis[87]. The lysis pathway also consists of another protein, antiholin that binds to holin and prevents holin from participating in hole formation[88,89]. Expressing antiholin in titratable amounts from a plasmid could be an interesting setup to experimentally investigate the role of decoys on intracellular event timing and connect these results with the theoretical foundation setup here.

Data availability

This research paper does not contain any experimental data. The results presented in the paper are theoretical and computational. All the details are given in the supplementary information file or/and in the method sections.

References

1. Klosin, A. et al. Phase separation provides a mechanism to reduce noise in cells. *Science* **367**, 464–468 (2020).
2. Venturelli, O. S., El-Samad, H. & Murray, R. M. Synergistic dual positive feedback loops established by molecular sequestration generate robust bimodal response. *Proc. Natl. Acad. Sci.* **109**, E3324–E3333 (2012).
3. Buchler, N. E. & Louis, M. Molecular titration and ultrasensitivity in regulatory networks. *J. Mol. Biol.* **384**, 1106–1119 (2008).
4. Wang, T., Tague, N., Whelan, S. A. & Dunlop, M. J. Programmable gene regulation for metabolic engineering using decoy transcription factor binding sites. *Nucleic Acids Res.* **49**, 1163–1172 (2021).
5. Gao, R. et al. A balancing act in transcription regulation by response regulators: Titration of transcription factor activity by decoy DNA binding sites. *Nucleic Acids Res.* **49**, 11537–11549 (2021).
6. Parab, L., Pal, S. & Dhar, R. Transcription factor binding process is the primary driver of noise in gene expression. *PLoS Genet.* **18**, 1–28 (2022).
7. Mann, M. J. Transcription factor decoys: A new model for disease intervention. *Ann. N. Y. Acad. Sci.* **1058**, 128–139 (2005).

8. Kemme, C. A., Nguyen, D., Chattopadhyay, A. & Iwahara, J. Regulation of transcription factors via natural decoys in genomic DNA. *Transcription* **7**, 115–120 (2016).
9. Schmidt, A. et al. The quantitative and condition-dependent *Escherichia coli* proteome. *Nat. Biotechnol.* **34**, 104–110 (2016).
10. Burger, A., Walczak, A. M. & Wolynes, P. G. Abduction and asylum in the lives of transcription factors. *Proc. Natl. Acad. Sci.* **107**, 4016–4021 (2010).
11. Burger, A., Walczak, A. M. & Wolynes, P. G. Influence of decoys on the noise and dynamics of gene expression. *Phys. Rev. E* **86**, 041920 (2012).
12. Soltani, M., Bokes, P., Fox, Z. & Singh, A. Nonspecific transcription factor binding can reduce noise in the expression of downstream proteins. *Phys. Biol.* **12**, 055002 (2015).
13. Dey, S., Soltani, M. & Singh, A. Enhancement of gene expression noise from transcription factor binding to genomic decoy sites. *Sci. Rep.* **10**, 9126 (2020).
14. Jayanthi, S. & Del Vecchio, D. Tuning genetic clocks employing DNA binding sites. *PLoS ONE* **7**, e41019 (2012).
15. Franco, E. et al. Timing molecular motion and production with a synthetic transcriptional clock. *Proc. Natl. Acad. Sci.* **108**, E784–E793 (2011).
16. Cuba Samaniego, C., Giordano, G., Kim, J., Blanchini, F. & Franco, E. Molecular titration promotes oscillations and bistability in minimal network models with monomeric regulators. *ACS Synth. Biol.* **5**, 321–333 (2016).
17. Dey, S. & Singh, A. Diverse role of decoys on emergence and precision of oscillations in a biomolecular clock. *Biophys. J* . **120**, 5564–5574 (2021).
18. Zhang, Z., Dey, S. & Singh, A. The impact of decoys on a genetic oscillator based on coupled positive-negative feedbacks. *IFAC-PapersOnLine* **55**, 127–132 (2022).
19. Das, S. & Choubey, S. Tunability enhancement of gene regulatory motifs through competition for regulatory protein resources. *Phys. Rev. E* **102**, 052410 (2020).
20. Ali, M. Z. & Brewster, R. C. Controlling gene expression timing through gene regulatory architecture. *PLoS Comput. Biol.* **18**, 1–21 (2022).
21. Fu, H., Xiao, F. & Jun, S. Bacterial replication initiation as precision control by protein counting. *PRX Life* **1**, 013011 (2023).
22. Gupta, S., Fancher, S., Korswagen, H. C. & Mugler, A. Temporal precision of molecular events with regulation and feedback. *Phys. Rev. E* **101**, 062420 (2020).
23. Dey, S., Kannoly, S., Bokes, P., Dennehy, J. J. & Singh, A. Feedforward genetic circuits regulate the precision of event timing. In *2021 European Control Conference (ECC)* 2127–2132 (IEEE, 2021).
24. Zheng, X.-D., Yang, X.-Q. & Tao, Y. Bistability, probability transition rate and first-passage time in an autoactivating positive-feedback loop. *PLoS ONE* **6**, e17104 (2011).
25. Rezaee, S., Nieto, C. & Singh, A. Optimizing precision in cellular clocks through self-regulated accumulation of molecules. In *2023 27th International Conference on System Theory, Control and Computing (ICSTCC)* 505–510 (IEEE, 2023).
26. Biswas, K. & Ghosh, A. Timing efficiency in small-RNA-regulated post-transcriptional processes. *Phys. Rev. E* **101**, 022418 (2020).
27. Biswas, K. & Ghosh, A. First passage time in post-transcriptional regulation by multiple small RNAs. *Eur. Phys. J. E* **44**, 1–10 (2021).
28. Biswas, K., Jolly, M. K. & Ghosh, A. First passage time properties of miRNA-mediated protein translation. *J. Theor. Biol.* **529**, 110863 (2021).
29. Ghusinga, K. R., Vargas-Garcia, C. A. & Singh, A. A mechanistic stochastic framework for regulating bacterial cell division. *Sci. Rep.* **6**, 30229 (2016).
30. Ghusinga, K. R., Dennehy, J. J. & Singh, A. First-passage time approach to controlling noise in the timing of intracellular events. *Proc. Natl. Acad. Sci.* **114**, 693–698 (2017).
31. Rijal, K., Prasad, A., Singh, A. & Das, D. Exact distribution of threshold crossing times for protein concentrations: Implication for biological timekeeping. *Phys. Rev. Lett.* **128**, 048101 (2022).
32. Singh, A. & Dennehy, J. J. Stochastic holin expression can account for lysis time variation in the bacteriophage λ. *J. R. Soc. Interface* **11**, 20140140 (2014).
33. Gupta, S., Varennes, J., Korswagen, H. C. & Mugler, A. Temporal precision of regulated gene expression. *PLoS Comput. Biol.* **14**, e1006201 (2018).
34. Charlebois, D. A., Abdennur, N. & Kaern, M. Gene expression noise facilitates adaptation and drug resistance independently of mutation. *Phys. Rev. Lett.* **107**, 218101 (2011).
35. Schuh, L. et al. Gene networks with transcriptional bursting recapitulate rare transient coordinated high expression states in cancer. *Cell Syst.* **10**, 363–378 (2020).
36. Vahdat, Z. & Singh, A. Frequency-dependent modulation of stochasticity in postsynaptic neuron firing times. In *2022 IEEE 61st Conference on Decision and Control (CDC)* 635–640 (IEEE, 2022).
37. Braun, W., Matthews, P. C. & Thul, R. First-passage times in integrate-and-fire neurons with stochastic thresholds. *Phys. Rev. E* **91**, 052701 (2015).
38. Suter, D. M. et al. Mammalian genes are transcribed with widely different bursting kinetics. *Science* **332**, 472–474 (2011).
39. Dar, R. D., Hosmane, N. N., Arkin, M. R., Siliciano, R. F. & Weinberger, L. S. Screening for noise in gene expression identifies drug synergies. *Science* **344**, 1392–1396 (2014).
40. Corrigan, A. M., Tunnacliffe, E., Cannon, D. & Chubb, J. R. A continuum model of transcriptional bursting. *eLife* **5**, e13051 (2016).
41. Dar, R. D. et al. Transcriptional burst frequency and burst size are equally modulated across the human genome. *Proc. Natl. Acad. Sci.* **109**, 17454–17459 (2012).
42. Pedraza, J. M. & Paulsson, J. Effects of molecular memory and bursting on fluctuations in gene expression. *Science* **319**, 339–343 (2008).
43. Kumar, N., Singh, A. & Kulkarni, R. V. Transcriptional bursting in gene expression: Analytical results for genera stochastic models. *PLoS Comput. Biol.* **11**, e1004292 (2015).
44. Singh, A. & Soltani, M. Quantifying intrinsic and extrinsic variability in stochastic gene expression models. *PLoS ONE* **8**, e84301 (2013).
45. Chong, S., Chen, C., Ge, H. & Xie, X. S. Mechanism of transcriptional bursting in bacteria. *Cell* **158**, 314–326 (2014).
46. Singh, A., Razooky, B., Cox, C. D., Simpson, M. L. & Weinberger, L. S. Transcriptional bursting from the HIV-1 promoter is a significant source of stochastic noise in HIV-1 gene expression. *Biophys. J* . **98**, L32–L34 (2010).
47. Singh, A. Transient changes in intercellular protein variability identify sources of noise in gene expression. *Biophys. J* . **107**, 2214–2220 (2014).
48. Golding, I., Paulsson, J., Zawilski, S. & Cox, E. Real-time kinetics of gene activity in individual bacteria. *Cell* **123**, 1025–1036 (2005).
49. Singh, A., Razooky, B. S., Dar, R. D. & Weinberger, L. S. Dynamics of protein noise can distinguish between alternate sources of gene-expression variability. *Mol. Syst. Biol.* **8**, 607 (2012).
50. Bartman, C. R., Hsu, S. C., Hsiung, C.C.-S., Raj, A. & Blobel, G. A. Enhancer regulation of transcriptional bursting parameters revealed by forced chromatin looping. *Mol. Cell* **62**, 237–247 (2016).
51. Shahrezaei, V. & Swain, P. S. Analytical distributions for stochastic gene expression. *Proc. Natl. Acad. Sci.* **105**, 17256–17261 (2008).
52. Thattai, M. & van Oudenaarden, A. Intrinsic noise in gene regulatory networks. *Proc. Natl. Acad. Sci.* **98**, 8614–8619 (2001).

53. Friedman, N., Cai, L. & Xie, X. Linking stochastic dynamics to population distribution: An analytical framework of gene expression. *Phys. Rev. Lett.* **97**, 168302 (2006).
54. Murugan, R. & Kreiman, G. On the minimization of fluctuations in the response times of autoregulatory gene networks. *Biophys. J*. **101**, 1297–1306 (2011).
55. Murugan, R. Theory of transcription bursting: Stochasticity in the transcription rates. *J. Math. Chem.* **58**, 2140–2187 (2020).
56. Shahrezaei, V. & Marguerat, S. Connecting growth with gene expression: Of noise and numbers. *Curr. Opin. Microbiol.* **25**, 127–135 (2015).
57. Yu, J., Xiao, J., Ren, X., Lao, K. & Xie, X. S. Probing gene expression in live cells, one protein molecule at a time. *Science* **311**, 1600–1603 (2006).
58. Paulsson, J. Model of stochastic gene expression. *Phys. Life Rev.* **2**, 157–175 (2005).
59. Pariat, M. et al. Proteolysis by calpains: A possible contribution to degradation of p53. *Mol. Cell. Biol.* **17**, 2806–2815 (1997).
60. Abu Hatoum, O. et al. Degradation of myogenic transcription factor MyoD by the ubiquitin pathway in vivo and in vitro: Regulation by specific DNA binding. *Mol. Cell. Biol.* **18**, 5670–5677 (1998).
61. Thomas, D. & Tyers, M. Transcriptional regulation: Kamikaze activators. *Curr. Biol.* **10**, R341–R343 (2000).
62. McQuarrie, D. A. Stochastic approach to chemical kinetics. *J. Appl. Phys.* **4**, 413–478 (1967).
63. Gillespie, D. T. Approximate accelerated stochastic simulation of chemically reacting systems. *J. Comput. Phys.* **115**, 1716–1733 (2001).
64. Gardiner, C. W. et al. *Handbook of Stochastic Methods* Vol. 4 (Springer, 1985).
65. Van Kampen, N. *Stochastic Processes in Physics and Chemistry* (Elsevier, 2011).
66. Elf, J. & Ehrenberg, M. Fast evaluation of fluctuations in biochemical networks with the linear noise approximation. *Genome Res.* **13**, 2475–2484 (2003).
67. Modi, S., Soltani, M. & Singh, A. Linear noise approximation for a class of piecewise deterministic Markov processes. In *2018 Annual American Control Conference (ACC)* 1993–1998 (2018).
68. Munsky, B., Hlavacek, W. S. & Tsimring, L. S. *Quantitative Biology: Theory, Computational Methods, and Models* (The MIT Press, 2018).
69. Thomas, P., Straube, A. V. & Grima, R. The slow-scale linear noise approximation: an accurate, reduced stochastic description of biochemical networks under timescale separation conditions. *BMC Syst. Biol.* **6**, 39 (2012).
70. Co, A. D., Lagomarsino, M. C., Caselle, M. & Osella, M. Stochastic timing in gene expression for simple regulatory strategies. *Nucleic Acids Res.* **45**, 1069–1078 (2016).
71. Kannoly, S. et al. Optimum threshold minimizes noise in timing of intracellular events. *iScience* **23**, 101186 (2020).
72. Alon, U. *An Introduction to Systems Biology: Design Principles of Biological Circuits* (Chapman and Hall/CRC, 2011).
73. Ochab-Marcinek, A., Jędrak, J. & Tabaka, M. Hill kinetics as a noise filter: The role of transcription factor autoregulation in gene cascades. *Phys. Chem. Chem. Phys.* **19**, 22580–22591 (2017).
74. Czuppon, P. & Pfaffelhuber, P. Limits of noise for autoregulated gene expression. *J. Math. Biol.* **77**, 1153–1191 (2018).
75. Sepúlveda, L. A., Xu, H., Zhang, J., Wang, M. & Golding, I. Measurement of gene regulation in individual cells reveals rapid switching between promoter states. *Science* **351**, 1218–1222 (2016).
76. Gillespie, D. T. Exact stochastic simulation of coupled chemical reactions. *J. Phys. Chem.* **81**, 2340–2361 (1977).
77. Hausser, J., Mayo, A., Keren, L. & Alon, U. Central dogma rates and the trade-off between precision and economy in gene expression. *Nat. Commun.* **10**, 68 (2019).
78. Denichenko, P. et al. Specific inhibition of splicing factor activity by decoy RNA oligonucleotides. *Nat. Commun.* **10**, 1590 (2019).
79. Hooykaas, M. J. et al. RNA accessibility impacts potency of tough decoy microRNA inhibitors. *RNA Biol.* **15**, 1410–1419 (2018).
80. Howard, J. M. et al. HNRNPA1 promotes recognition of splice site decoys by U2AF2 in vivo. *Genome Res.* **28**, 689–698 (2018).
81. Luo, L., Bai, Y. & Fu, X. Stochastic threshold in cell size control. *Phys. Rev. Res.* **5**, 013173 (2023).
82. Soltani, M., Vargas-Garcia, C. A., Antunes, D. & Singh, A. Intercellular variability in protein levels from stochastic expression and noisy cell cycle processes. *PLoS Comput. Biol.* **12**, e1004972 (2016).
83. Cao, Z. & Grima, R. Analytical distributions for detailed models of stochastic gene expression in eukaryotic cells. *Proc. Natl. Acad. Sci.* **117**, 4682–4692 (2020).
84. Niranjani, G. & Murugan, R. Generalized theory on the mechanism of site-specific DNA-protein interactions. *J. Stat. Mech. Theory Exp.* **2016**, 053501 (2016).
85. El-Samad, H., Kurata, H., Doyle, J. C., Gross, C. A. & Khammash, M. Surviving heat shock: Control strategies for robustness and performance. *Proc. Natl. Acad. Sci.* **102**, 2736–2741 (2005).
86. Feder, Z. A. et al. Subcellular localization of the J-protein Sis1 regulates the heat shock response. *J. Cell Biol.* **220**, e202005165 (2020).
87. Kannoly, S., Singh, A. & Dennehy, J. J. An optimal lysis time maximizes bacteriophage fitness in quasi-continuous culture. *MBio* **13**, e03593 (2022).
88. Cahill, J. et al. Spatial and temporal control of lysis by the lambda holin. *MBio* **15**, e01290 (2024).
89. White, R., Tran, T. A. T., Dankenbring, C. A., Deaton, J. & Young, R. The n-terminal transmembrane domain of λ s is required for holin but not antiholin function. *J. Bacteriol.* **192**, 725–733 (2010).

Author contributions

K.B., S.D., and A.S. designed the project and contributed to developing analytical tools. K.B. performed the necessary computations. The authors discussed the results and collaborated on the writing, read, and approved the final manuscript.

Declarations

Competing interests
The authors declare no competing interests.

Additional information